EXPERIMENTAL AND NUMERICAL STUDY ON MELTING PROCESS OF PARAFFIN IN A VERTICAL ANNULAR CYLINDER

by

Yangli CHEN, Changhong PENG, and Yun GUO*

School of Nuclear Science and Technology, University of Science and Technology of China, Hefei, China

Original scientific paper
https://doi.org/10.2298/TSCI160504099C

The melting process of paraffin wax in a central heating vertical annular cylinder was simulated by a numerical model based on the enthalpy-porosity method. The numerical results were validated against the experimental results. The melting experiment was performed in a thermostatic water tank which can provide good initial conditions and constant temperature boundary conditions. The electrical heating rod located in the central of the cylinder was supposed to provide heating at a constant power. Good agreements between experimental and numerical heat transfer data were achieved. Natural convection and melt front interface were well predicted by simulation. However, considerable differences appeared due to mushy zone constant in the model. A recommended value of mushy zone constant was obtained by comparison to the experiment. The influence of thermal conductivity coefficient was also analyzed numerically.

Key words: *melting process, enthalpy-porosity method, numerical simulation, phase change experiments, mushy zone constant*

Introduction

The melting process is an important part of many manufacturing process like crystal growth and casting. Thermal storage systems which use the latent heat of phase change materials (PCM) also take the advantage of melting process. Besides, severe accidents in nuclear reactors involve with the fuel melting. Thus the experiments on natural convection and thermal transfer phenomena during melting process and the development of numerical simulation models are of significant importance.

Quite a lot of experiments have been carried out at various configurations towards efficient energy storage. The common shapes of the containers are rectangular cavities, spherical capsules, tubes or cylinders (vertical and horizontal). Different heating conditions such as isothermal heating and constant heat flux are also applied. Zhang *et al*. [1] conducted experiments about the melting process of n-octadecane ($C_{18}H_{38}$) held in a rectangular enclosure with one wall heated by discrete sources at a constant rate and other surfaces being adiabatic. Tan [2] investigated experimentally the melting of n-octadecane inside a sphere for multiple wall temperatures and subcooling ranges. Sparrow and Broadbent [3] presented experimental study for melting of n-eicosane in a vertical tube heated isothermally from its side. Hosseini *et al*. [4]

* Corresponding author, e-mail: guoyun79@ustc.edu.cn

carried out experiments to evaluate the role of buoyancy-driven convection during constrained melting of PCM inside a shell and tube heat exchanger.

Various techniques have been used in the development of models that describe heat transfer and the interface evolution during melting process. The main difficulty of the models lies in the two-phase interface tracking. Basically, two kinds of methods: particle methods and grid methods are usually implemented to fix this problem. As for particle methods, for instance, Zhao *et al*. [5] presented a method to simulate the melting and flowing phenomena with different materials in multiple phases based on a modified lattice Boltzmann method. Carlson [6] developed a fast and stable system for animating materials like wax, glass, and water that melt, flow, and solidify with a modification of the Marker-and-Cell algorithm. The grid methods can be classified into two groups: moving grid method and fixed grid methods. Jana *et al*. [7] introduced a numerical model using moving grids, which was good at the prediction of a sharp melting/solidification front. The moving grid methods give high accuracy in predicting the interface position, but it is more complicated than the fixed grid methods, especially in case of complex shape of interface, special attention must be paid to the deformation of elements. Uchibori and Ohshima [8] applied the extended finite element method, a fixed-mesh-method, to evaluating the melting/solidification process appearing in the nuclear fuel cycle. The enthalpy method developed by Voller *et al*. [9] is also based on fixed grid to solve phase change problems.

The present study attempts to provide the results of an experiment of paraffin wax melting in a central heating vertical annular cylinder as a validation to the enthalpy-porosity method [10], an extended enthalpy method that is applicable for melting over a temperature range. The enthalpy-porosity method is quite popular because re-meshing is not required. In addition, there is only one energy equation during the calculation, thus there is no need to consider the boundary conditions at the solid-liquid interface. The objective of the current study is achieved by a combined approach which includes an experiment and a complete numerical solution. The numerical simulation was performed on ANSYS FLUENT software. The analysis of numerical results has been conducted, and the influence of the mushy zone constant, C, to the melting front evolution has been investigated.

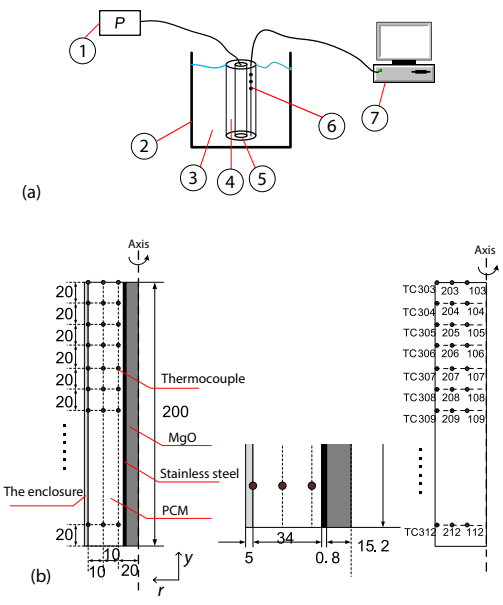

Figure 1. Experimental configuration (all dimensions in mm); *1 – power, 2 – thermostatic water tank, 3 – water, 4 – PCM, 5 – electrical heating rod, 6 – thermocouple, 7 – data collection system*

Experimental investigation

Experimental set-up

Experiments were carried out to validate the numerical model of melting in a central heating vertical annular cylinder. The structure of the experiment, fig. 1(a) included a heating system, a water bath system, and a temperature measurement system. Before starting the experiment, an electrical heating rod was located in the axis of the enclosure with bottom and top fixed, and thermocouples (TC) were placed in the PCM domain, as shown in fig. 1(b). Then molten PCM was poured in the enclosure 2 cm

layers each time, allowing the earlier layer to solidify, to ensure no air bubbles in the PCM. The final height of the PCM was 20 cm, which was shorter than the height of the enclosure 25 cm, considering the volume expansion of PCM during experiment progression. The enclosure was then placed into the thermostatic water tank in order to have an initial temperature of the whole experimental domain. The experiments were subsequently conducted with all TC showing temperature of 323.15 K (50 °C) uniformly within 2 K, and the electrical heating rod started to provide power at a constant level which was controlled by a transformer. The water bath continued to provide isothermal boundary condition of 313.15 K throughout the experimental progression. Tests were performed at 100 W, 150 W, and 200 W, separately.

The paraffin wax used in the current investigation is a mixture, whose phase-transient temperature is a range. By using differential scanning calorimetry, the melting and solidification temperatures were obtained (58 °C and 56 °C). Properties of the paraffin wax are listed in tab. 1. The radius of the electrical heating rod is 16 mm. In terms of the components of the rod, stainless steel (thickness = 0.8 mm) is served as the boundary of the rod, and enclosed part is filled with magnesium oxide (MgO) powder for power dissipating. Thermal resistance wires disperse in MgO powder. The properties of stainless steel and MgO are listed in tab. 1. The enclosure (thickness = 5mm) of the PCM is made from plastic, whose properties are also listed in tab. 1. The inner diameter of the enclosure is 8 cm.

Table 1. Physical properties

Properties (units)	Solid paraffin	Liquid paraffin	MgO	Stainless steel	Enclosure material
Density, [kgm^{-3}]	900	900	3580	8030	1180
Thermal conductivity, [Wm^{-1}K^{-1}]	0.25	0.25	60	16.2	0.19
Specific heat capacity, [Jkg^{-1}K^{-1}]	6600	2600	800	502.5	1225
Dynamic viscosity, [kgm^{-1}s^{-1}]	–	0.004	–	–	–
Volume expansion coefficient, [K^{-1}]	–	0.001	–	–	–
Latent heat, [Jkg^{-1}]	–	210000	–	–	–

Experimental results

As a result, fig. 2(a) compares the variations of temperature at different height at radius = 2 cm, for a power level of 100 W. The locations of the TC were quite close to the heating rod, the distance of which was only 0.4 cm. Initially, the temperatures increased at various heights, and all exceeded the melting point in the early time. That means the initial stage of PCM melting was not concerned with height, when the heat transfer was driven by conduction mainly. As the effects of convection became dominant, the temperature became various along different height due to the heated flow driven by natural convection near the heating wall. What can be noted is that there was a period of time when the temperature stayed stable during temperature rising, and it seems to last longer when the location of the TC was lower. This phenomenon will be discussed in this paper later.

Figure 2(b) shows the temperature variations at radius = 3 cm, which is the middle of the PCM. The initial temperature in this figure was not influenced by conduction. The inner material needed to absorb power to heat itself. So the temperature remained steady at first, and afterwards a quick rise was observed. This indicated the time of arrival of the solid/liquid interface at these points at radius = 3 cm. During temperature rising, the stable periods still existed but not so obviously.

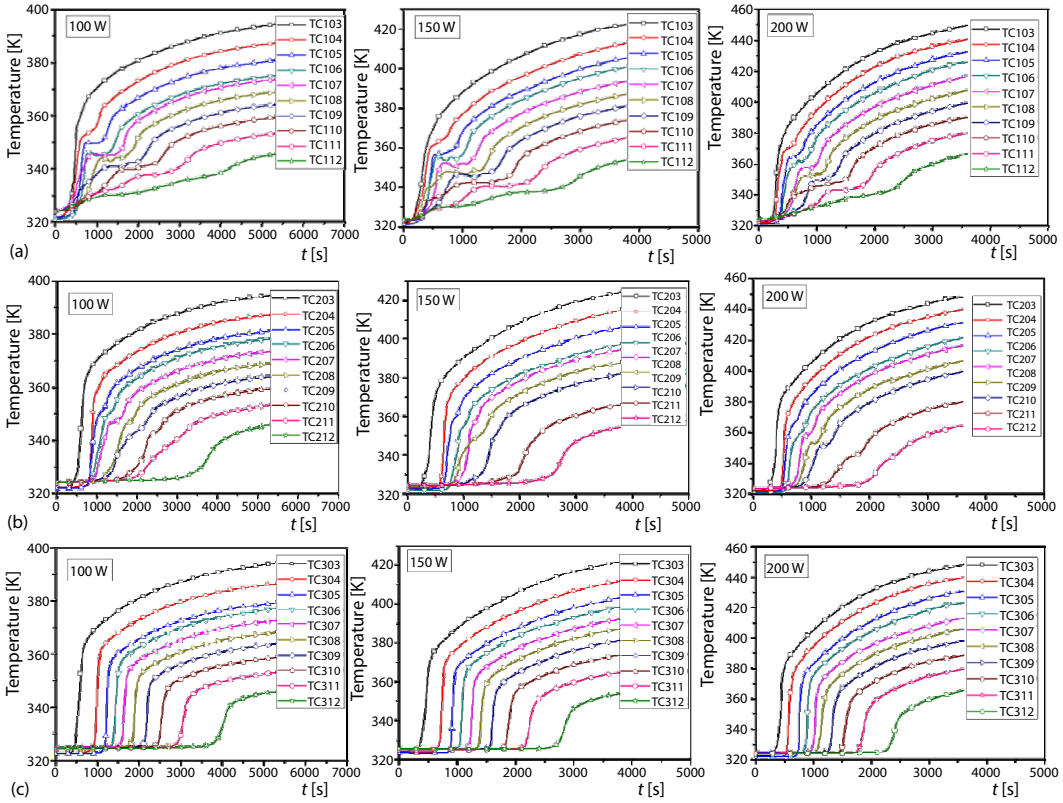

Figure 2. Temperature variations; (a) radius = 2 cm, (b) radius = 3 cm, and (c) radius = 4 cm

Figure 2(c) illustrates the temperature variations at radius = 4 cm, near the enclosure wall. The temperature variations were similar to the trend in fig. 2(b), except that there was no sign of stable period when temperature rising in fig. 2(c).

Numerical model

In the enthalpy-porosity method, the energy equation is written in terms of sensible enthalpy instead of temperature. Therefore, the latent heat is treated as enthalpy rise. During the calculating process, the phase of the PCM is distinguished by the enthalpy calculated in the whole computational domain without tracking the phase change interface explicitly. However, there is a problem coming up that is how to make the velocity of the solid zone equals zero since the same momentum equation is solved in the entire computational domain. A concept called mushy zone was proposed, and it treats the zone where the temperature is between the solidification point, T_{sol}, and the melting point, T_{liq}, as a porous zone. The velocity is dragged in the porous zone and becoming slower. Solid zone is where the porosity equals one, thus the velocity of solid zone nearly equals zero.

The governing conservation equations are listed:

$$\frac{\partial \rho}{\partial t} + \nabla(\rho \vec{u}) = 0 \tag{1}$$

$$\frac{\partial \rho}{\partial t}(\rho u) + \nabla(\rho \vec{u} u) = \nabla(\mu \nabla u) - \frac{\partial P}{\partial x} + Au \tag{2}$$

$$\frac{\partial}{\partial t}(\rho v)+\nabla(\rho\vec{u}v)=\nabla(\mu\nabla v)-\frac{\partial P}{\partial y}+Av+S_b \tag{3}$$

$$\frac{\partial}{\partial t}(\rho h)+\nabla(\rho\vec{u}h)=\nabla(\alpha\nabla h)+S_h \tag{4}$$

where $\vec{u}=(u, v)$ is the velocity vector and A is the term that controls the velocity in the mushy zone and solid zone. The definition of it mimics the Carman-Kozeny equations for flow in a porous media.

$$A=-\frac{C(1-\beta)^2}{\beta^3+b} \tag{5}$$

where $b = 0.001$ is just a constant in order to avoid denominator equaling zero, and C is mushy zone constant which is the only changeable parameter in the melting/solidification model of ANSYS FLUENT. The density of PCM decreases during the melting process when the temperature rises. Therefore, the Boussinesq approximation is implemented into this method that density of PCM is treated as constant, and the thermal expansion coefficient, α_v, is only used in the gravity source term S_b.

$$S_b=\frac{\rho_{\text{ref}}\,\text{g}\,\alpha_v(h-h_{\text{ref}})}{c_p} \tag{6}$$

The latent heat is accounted for on defining the energy equation source term:

$$S_h=\frac{\partial}{\partial t}(\rho\Delta H)+\nabla(\rho\vec{u}\Delta H) \tag{7}$$

where $\Delta H = \beta L$, and the definition of β is:

$$\beta=\begin{cases}0 & T<T_{\text{sol}}\\ (T-T_{\text{sol}})/(T_{\text{liq}}-T_{\text{sol}}) & T_{\text{sol}}<T<T_{\text{liq}}\\ 1 & T>T_{\text{liq}}\end{cases} \tag{8}$$

Numerical simulation

Axial symmetry of the physical model was assumed for the computational domain presented in fig. 1(b). For the properties during the calculation, it was assumed that both solid and liquid phases were homogeneous and isotropic, and the melting process was axisymmetric. The molten PCM was incompressible Newtonian fluids, and laminar flow was assumed in natural convection. The power imposed to the heating rob was treated as volume heat flux of the entire volume of MgO powder. Providing that the thermostatic water tank kept the boundary of experiment cell at a constant temperature ($T_o = 323.15$ K), and the bottom and top of the heating rod was adiabatic. Thus the boundary conditions for the computational domain are listed in fig. 3. The initial temperature of the entire computational domain is $T_{\text{ini}} = 323.15$ K.

A 2-D model was built with structured grids. A grid sensitivity study was done by using 8400, 15500, and 32800 grids with the first layer of 0.2 mm. The time-wise melt fraction result is shown

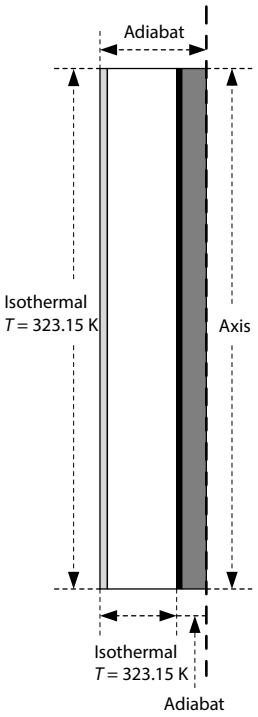

Figure 3. Boundary conditions for simulation

in fig. 4(a), and the difference between 8400 and 15500, 15500 and 32800 grids is illustrated in fig. 4(b). Based on these results, the 15500 grids were chosen for all computations. The pressure-velocity coupling scheme was SIMPLE, and the pressure discretization scheme was standard. Convergence of the solution was checked at each time step, with the convergence criterion of 10^{-3} for the continuity, 10^{-5} for velocity components, and 10^{-6} for energy. The time step in the calculation was 0.1 second. It took nearly a week of computing with an Intel core i5-3450 CPU at 3.10 GHz and 3.88 G of RAM.

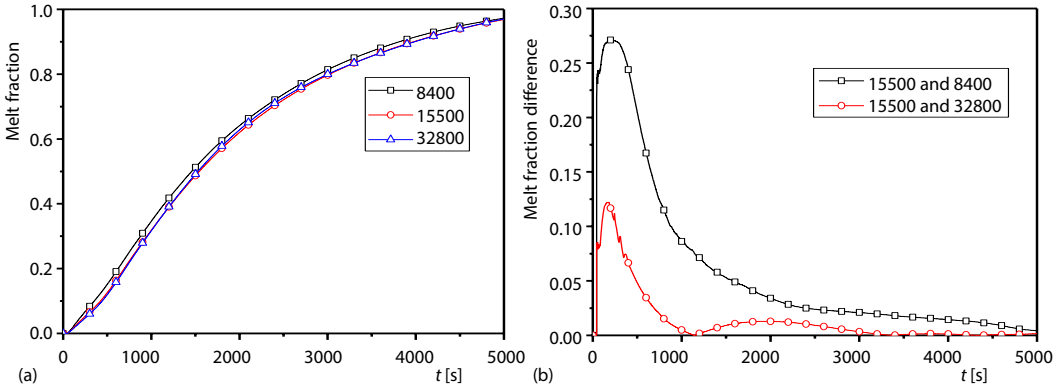

Figure 4. Grid sensitivity; (a) melt fraction variations, (b) melt fraction difference variations

The significance of the enclosure to the simulation results was analyzed. If the enclosure part was not included in the computational domain, a steady-state would be reached in the simulation results. Figure 5 compares the melt fraction under the simulation conditions with and without the enclosure. The steady-state of the non-enclosure condition started at about 3500 seconds. The melt front evolution without the enclosure is shown in fig. 6 (red for liquid paraffin and blue for solid paraffin). Compared with fig. 9 (melt front evolution with the enclosure), it is clear that the thermal resistance of the enclosure is of important significance to the heat transfer process during the simulation of melting.

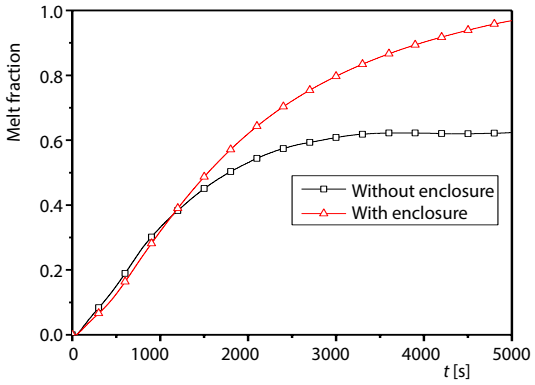

Figure 5. Comparison of melt fraction

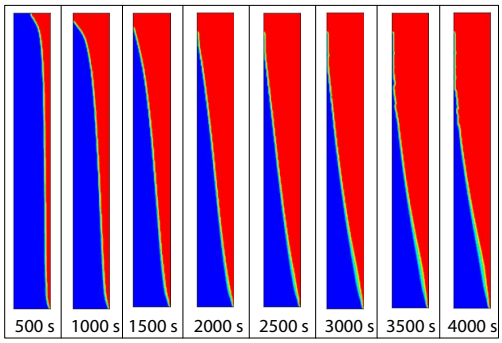

Figure 6. Melt front evolution of simulation without the enclosure

The mushy zone constant, C, in the momentum equation is a significant parameter for accurately modeling phase change phenomena. It reflects the kinetic process in the mushy

zone and the solid zone of the model, thus it affects the melting progression in the simulation. The $C = 10^5$-10^7 is recommended by ANSYS FLUENT [11], also $C = 10^8$ is recommended by Shmueli [12] in melting in a vertical cylindrical tube. According to Kheirabad and Groulx [13], higher C values correspond to delay melting of PCM. In the present study, the effectiveness of C is analyzed in terms of velocity, melt fraction, and temperature of PCM. The values of C investigated in this study are 10^5, 10^6, 10^7, and 10^8, with the power of 100 W.

Figure 7 compares the velocity variations using different values of C. As a damping term, C made the velocity of the solid regions pretty slow, and it shows that for every increase in C by a factor of 10, the value of velocity within the solid zone was decreased by a factor of 0.1. Then the velocity increased when the melting interface arrived. Finally the velocity remained stable, and the stable velocity was not related to the value of C. As can see from fig. 7(a), PCM began to melt early when $C = 10^5$ at higher height (18 cm). However, PCM seemed to delay melting when $C = 10^5$ at a lower height (6 cm), shown in fig. 7(c). That means small values of C can promote natural convection, bringing more heat to the upper zone, accelerating the melting progression of PCM at higher places and slowing down the melting process at lower place.

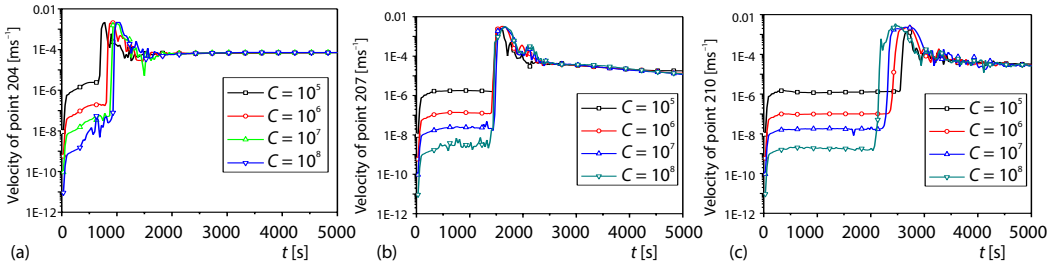

Figure 7. Velocities variations at radius = 2 cm; (a) height = 18 cm, (b) height = 12cm, and (c) height=6cm

Figure 8 presents the simulated melt fractions for different values of C. One can see from the figure that few differences can be found in melt fraction between values of C. Therefore, in the melting process of a central heating cylinder, C can barely affect the melt fraction. However, C dose affect the melt front evolution, as shown in fig. 9. Compared the shape of the liquid (shown in red) at various stages of melting in simulation, one can see that the influence of natural convection is more obvious when the value of C is smaller.

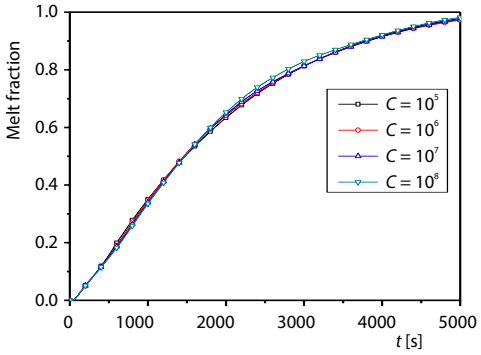

Figure 8. Melt fraction variations

The temperature of the PCM would rise unless stable-state has been reached. According to the temperature data of the experiment, stable-state does not exist in this experimental condition. Figure 10 shows the simulated variations of maximum temperature of the PCM region with time. At the early stage, heat transfer was controlled by conduction, therefore temperature increased sharply. Then came into a stage where conduction transferred into natural convection. Finally, natural convection became dominant. The rate of temperature rise became slow, and one can see that it entered into the convection stage early when $C = 10^5$. In order to find a proper mushy zone constant, C, that better simulates the experimental condition in this study, temperature data of TC 203,

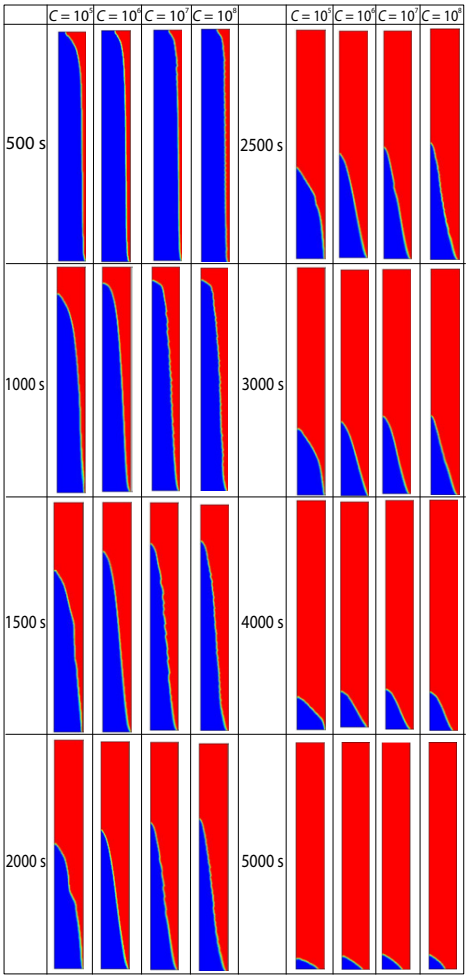

Figure 9. Melt front evolution (red for liquid, blue for solid) (*for color image see journal web site*)

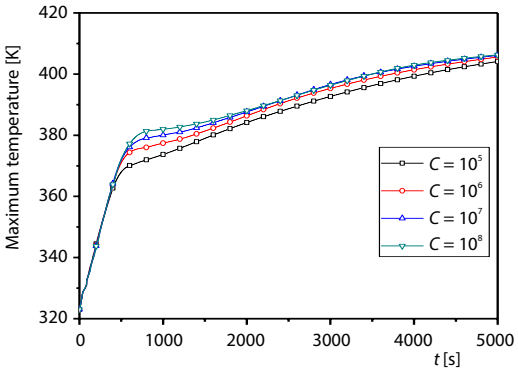

Figure 10. Maximum temperature of the PCM region *vs.* time

204, 303, and 304 were chosen to compare with the simulation results, as shown in fig. 11. The reason why the previously mentioned TC were selected is that they are at the top of the PCM region, where can be affected by natural convection at early time. The temperature evolution in fig. 11 illustrates that the simulation with $C = 10^6$ matched the experimental data most, especially at TC204. During last 2000, simulated values were generally larger than experimental, and that was caused by the accumulation of thermal losses in the experiment. Figure 12 compares the computational and experimental results with $C = 10^6$. The simulation described the melting process well at higher locations of the PCM, however, at lower places melting process in simulation was later than the realistic condition.

Other than power level of 100 W, tests under 150 W and 200 W also proved that $C = 10^6$ was suitable in this study, shown in fig. 13.

With $C = 10^6$, sensitivity analysis was conducted. In order to find the causes to the phenomena of temperature stable periods shown in fig. 2(a), properties of the paraffin wax during the numerical simulation were changed for discussion. The temperature variation results of numerical simulation in fig. 14(a) were with authentic properties used for comparison. When increasing the thermal conductivity of the paraffin wax to 20 W/mK, the temperature variations turned into fig. 14(b), where the temperature stable periods still existed. When increasing both thermal conductivity to 20 W/m·K and viscosity to 2 kg/ms, temperature variations depicted in fig. 14(c), there was no temperature stable period anymore. Under this computational condition of fig. 14(c), the paraffin wax melt totally at 1178 seconds, and the melting process was basically driven by thermal conduction. Therefore, one can say that it was the natural convection that caused the phenomena of temperature stable period. The heat flux was brought to the upper zone due to the natural convection, thus temperature remained stable temporarily at some points.

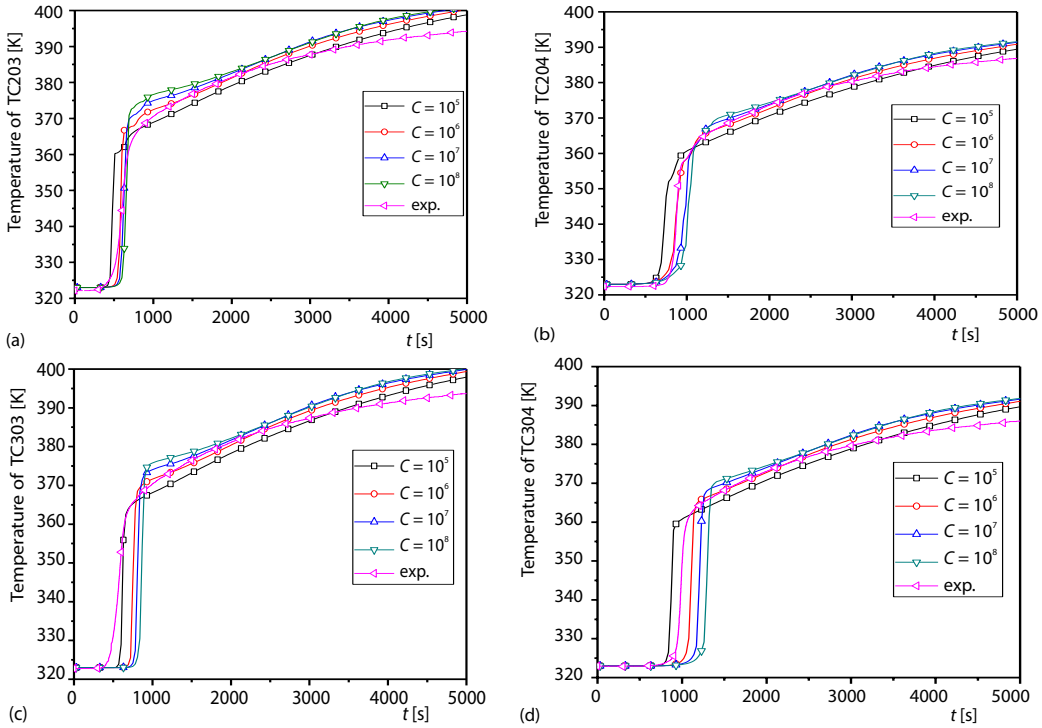

Figure 11. Temperature evolutions at different *C*; (a) TC 203, (b) TC 204, (c) TC 303, and (d) TC 304

Thermal conductivity is of significance to the melting progression. Different thermal conductivity *(k* = 0.2, 0.25, 0.3 W/mK) were applied in the simulation to analyze the effectiveness. Figure 15 compares melt fractions with time at different thermal conductivities under a power level of 200 W. According to the simulation results, the speed on melting of PCM was faster when k = 0.3 W/m·K. Compared with k = 0.25 W/m·K, it saved 6% of the time for entire melting when k = 0.3 W/m·K. Furthermore, the maximum temperature of PCM, shown in fig. 16, at k = 0.3 W/m·K was approximately 9 K lower than the simulation with k = 0.25 W/mK after natural convection built up. Therefore, larger values of the thermal conductivity coefficients

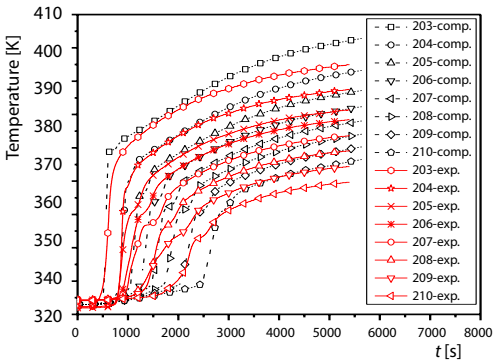

Figure 12. Comparison of temperature between experiment and simulation with $C = 10^6$

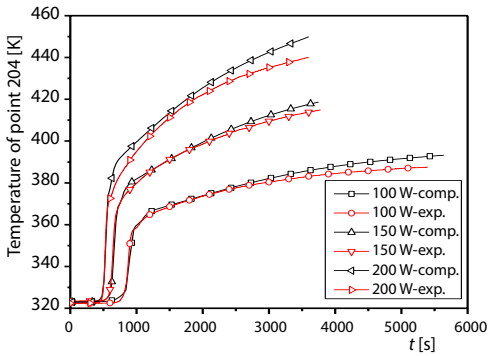

Figure 13. Comparison of temperature at different power level

contribute to reducing the increase of the maximum temperature during melting process. The material with larger thermal conductivity benefits decreasing the maximum temperature during melting.

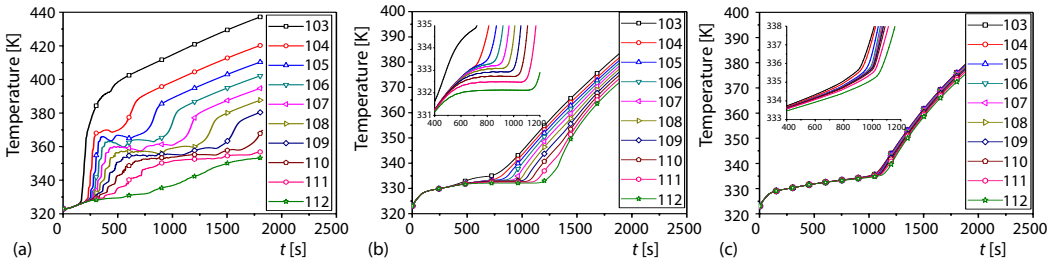

Figure 14. Temperature variations of different height at radius = 2 cm; (a) authentic properties, (b) thermal conductivity = 20 W/mK, and (c) thermal conductivity = 20 W/mK and viscosity = 2 kg/ms

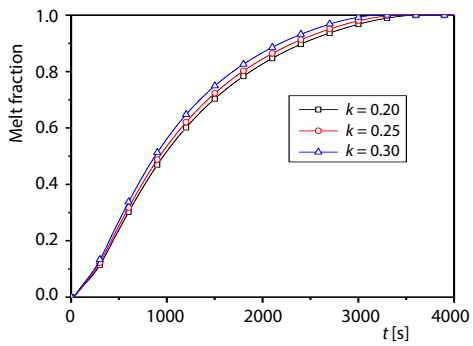

Figure 15. Comparison of melt fraction under different thermal conductivities

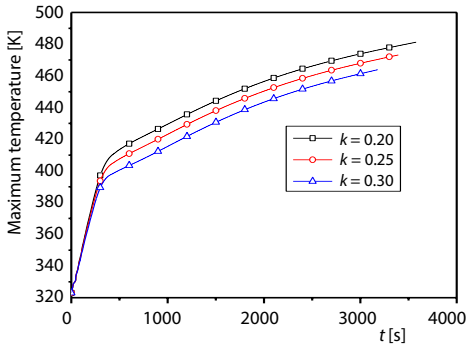

Figure 16. Comparison of maximum temperatures under different thermal conductivities

Conclusions

This paper described an experimental and computational study of PCM melting in a central heating annular cylinder with constant heat flux source and constant temperature water bath outside of the enclosure. The numerical simulation was carried out using an enthalpy-porosity method. Agreements were obtained in temperature variations.

The experiments provided temperature data at different levels of power. Comparing the temperature evolution along the radius, the temperature rise where near the heating rod was mainly controlled by conduction at the early stage. Later on, heat transfer over the upper part of the PCM was promoted after buoyancy induced natural convection was built.

During the simulated calculation, the effectiveness of mushy zone constant, C, was analyzed in terms of velocity, melt fraction, and temperature. It turns out that small values of C contribute to the building of natural convection. Also the effect of natural convection tends to be obvious when C is small. In order to find a suitable mushy zone constant to simulate the melting process under the experimental condition, temperature details obtained by numerical simulation were compared with experiment data. As a result, $C = 10^6$ was recommended, and quantitative agreements were achieved, which was also validated at different power levels. Moreover, through the discussion of changing the properties of paraffin wax, results showed that it was the natural convection that caused the phenomena of temperature stable period during the tempera-

ture variations where near the heating rod. The influence of thermal conductivity to the melting progression was also analyzed, and it is predicted that larger thermal conductivity accelerates the melting process and decreases the maximum temperature.

Acknowledgment

The author thanks to the project HT-ZDSY-09-2015002 cooperated with NPIC.

Nomenclature

b – constant, [–]
C – mushy zone constant, [–]
c_p – specific heat capacity, [Jkg^{-1}K^{-1}]
g – gravitational acceleration, [ms^{-2}]
h – enthalpy, [Jkg^{-1}]
k – thermal conductivity, [Wm^{-1}K^{-1}]
L – latent heat, [Jkg^{-1}]
P – pressure, [Pa]
T – temperature, [K]
t – time, [s]
u – velocity component in x-direction, [m^{-1}]
v – velocity component in y-direction, [ms^{-1}]
x – horizontal co-ordinate, [m]
y – vertical co-ordinate, [m]

Greek symbols

α – thermal diffusivity, [m^{2}s^{-1}]
α_v – thermal expansion coefficient, [K^{-1}]
β – liquid fraction, [–]
ρ – density, [kgm^{-3}]
μ – dynamic viscosity, [kgm^{-1}s^{-1}]

Subscripts

ini – initial
liq – liquid point
o – outer boundary
ref – reference state
sol – solid point

References

[1] Zhang, Y., *et al*., Melting in an Enclosure with Discrete Heating at a Constant Rate, *Experimental Thermal and Fluid Science , 6* (1999), 2, pp. 196-201
[2] Tan, F. L., Constrained and Unconstrained Melting inside a Sphere, *International Communications in Heat and Mass Transfer, 35* (2008), 4, pp. 466-475
[3] Sparrow, E. M., Broadbent J. A., Inward Melting in a Vertical Tube which Allows Free Expansion of the Phase-change Medium, *ASME. J. Heat Transfer, 104* (1982), 2, pp. 309-315
[4] Hosseini, M. J., *et al*., A Combined Experimental and Computational Study on the Melting Behavior of a Medium Temperature Phase Change Storage Material inside Shell and Tube Heat Exchanger, *International Communications in Heat and Mass Transfer, 39* (2012), 9, pp. 1416-1424
[5] Zhao, Y., *et al*., Melting and Flowing in Multiphase Environment, *Computers and Graphics, 30* (2006), 4, pp. 519-528
[6] Carlson, M. T., Rigid Melting and Flowing, Ph. D. thesis, Georgia Institute of Technology, Atlanta, Geo., USA, 2004
[7] Jana, S., *et al*., A Numerical Method to Compute Solidification and Melting Processes, *Applied Mathematical Modelling, 31* (2007), 1, pp. 93-119
[8] Uchibori, A., Ohshima, H., Numerical Analysis of Melting/Solidification Phenomena Using a Moving Boundary Analysis Method X-FEM, *Nuclear Technology, 167* (2009), 1, pp. 83-94
[9] Voller, V. R., *et al*., An Enthalpy Method for Convection/Diffusion Phase Change, *Int. J. Numer. Methods Eng, 24* (1987), 1, pp. 271-284
[10] Brent, D., *et al*., Enthalpy-Porosity Technique for Modeling Convection Diffusion Phase Change Application to the Melting of a Pure Metal, *Numerical Heat Transfer, 13* (1998), 3, pp. 297-318
[11] ***, ANASYS 14.5 Help. ANSYS, Inc., Canonsburg, Penn., USA, 2012
[12] Shmueli, H., *et al*., Melting in a Vertical Cylindrical Tube Numerical Investigation and Comparison with Experiments, *International Journal of Heat and Mass Transfer, 53* (2010), 19-20, pp. 4082-4091
[13] Kheirabadi, A. C., Groulx, D., The Effect of the Mushy-Zone Constant on Simulated Phase Change Heat Transfer, *Proceedings*, CHT-15: ICHMT International Symposium on Advances in Computational Heat Transfer, Piscataway, N. J., USA, 2015

Paper submitted: May 4, 2016
Paper revised: March 8, 2018
Paper accepted: March 23, 2018